A Forward Model for the Stratospheric Wind Interferometer For Transport Studies

D.S. Turner†, Yves J Rochon†, Ian C McDade‡ & Peyman Rahnama ‡

† *Atmospheric Science and Technology Directorate*
Environment Canada, Toronto, Ontario, Canada
‡ *York University, Toronto, Ontario, Canada*

Introduction

It is generally recognized that there is an urgent need for information about global wind distributions in the stratosphere. However, very few direct measurements exist. The High Resolution Doppler Imager instrument (HRDI) on the UARS spacecraft (Ortland et al, 1996) measured daytime stratospheric winds using Doppler shifts in scattered sunlight O_2 absorption features. On the same spacecraft the WIND Imaging Interferometer (WINDII, Shepherd et al, 1993) made daytime and night time measurements of the mesospheric and thermospheric winds, between 80 and 300 km, by observing Doppler shifts in visible airglow emission features. The aim of the Stratospheric Wind Interferometer For Transport (SWIFT) studies is to extend the WINDII observational technique into the stratosphere and provide global measurements of horizontal wind profiles between 15 and 55 km under both day and night time conditions.

SWIFT employs the same techniques as WINDII, that is— phase stepping interferometry, field widening of the Michelson interferometer, and imaging. However SWIFT will operate in the infrared region using a relatively isolated ozone thermal emission line. The main objectives of SWIFT (Shepherd et al, 2001; McDade et al, 2002) are the simultaneous measurement of horizontal wind velocity vectors and ozone concentration in the stratosphere during day and night which are essential for understanding global stratospheric dynamics and studies of ozone transport. Profiles in wind and ozone amounts are to be extracted from simultaneous measurements with a target accuracy of ±3m/s and ±5% respectively between 20 and 45km. This implies accuracy requirements along the line of sight wind before inversion of about ±1m/s.

The Atmospheric Science and Technology Branch has embarked on a project to study the feasibility of operationally assimilating SWIFT wind data into their numerical weather prediction model (NWP). In order to assimilate these data a fast forward model and gradient, or tangent linear/adjoint model is required. These models must be accurate in order to simulate an interferogram which is sensitive to wavenumber dependent variables. The current target for the maximum error allowed in the forward model is 20% of the aforementioned total error, that is— .2m/s.

The following pages offer a brief overview of; the history, the instrument, and the wind recovery algorithms, and preliminary results towards defining the forward model parameters. The work is an extension of the previous work done by Rochon et al (2006) and Rahnama et al (2006), which was primarily aimed at simulating the expected observations of SWIFT and its signal-to-noise ratio, optimize instrument design and assess instrument performance, and to quantify the expected SWIFT wind and ozone errors.

Brief History and Current Status of SWIFT

SWIFT was originally proposed to the European Space Agency (ESA) as an Earth Explorer Opportunity Mission in November 1998 by a Canadian team led by Gordon Shepherd of York University. ESA short-listed SWIFT as one of the top 5 candidate missions out of 27 international proposals (SWIFT was the highest ranking atmospheric mission in this competition). Later, ESA and the CSA investigated alternative launch opportunities for SWIFT throughout 2004. In late 2004, the CSA elected to make SWIFT the primary instrument for their next SciSat mission. In early 2005, the CSA selected a second partner instrument ARGO (a GPS occultation experiment) to accompany SWIFT on their new mission now named Chinook.

Chinook is just about to enter the Mission Phase A/B stage with a scheduled launch in late 2010 for a projected minimum 2 year mission.

Principle of Measurement

A small Doppler shift caused by the wind is measured by isolating an emission line from the limb emission spectrum using a narrowband filter and is projected through a field-widened Michelson interferometer to obtain an interferogram. The Doppler shift, $\delta\tilde{\nu}$, resulting from the wind is measured as a phase shift, $\delta\varphi$, of the interferogram; ie,

$$\delta\tilde{\nu} = \tilde{\nu}_0 v_w / c \text{ and } \delta\varphi = 2\pi\Delta\tilde{\nu}_0 \qquad \text{(1a \& 1b)}$$

where $\tilde{\upsilon}_o$ is the reference wavenumber at line centre, c is the speed of light, en vacua, and Δ is the optical path difference between the two arms of the Michelson interferometer. The impact of this shift is shown in Fig 1.

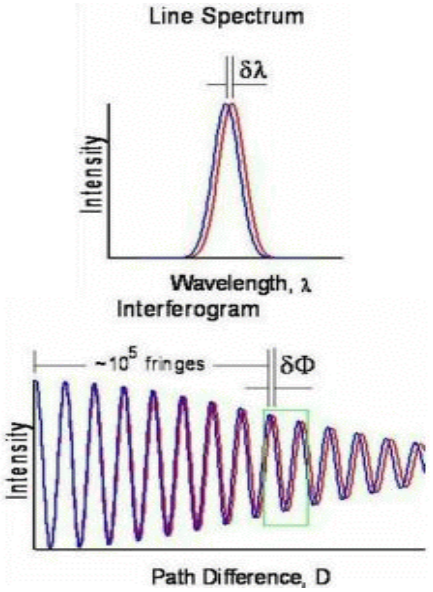

Fig 1: schematic of Doppler shift (top) resulting in a phase shift in the interferogram (bottom)

A wind measurement accuracy of 1m/s seems unrealistic as the Doppler shift is about 4×10^{-8} (cm^{-1}) for a line at 1133 (cm^{-1}). One can greatly improve the situation by measuring the phase shift at a high order fringe, that is— a large optical difference. This is accomplished by designing the Michelson with a fixed optical path difference of 18cm. Combining the Eqs 1a and b, leads to

$$\frac{\delta\varphi}{2\pi} = \tilde{\nu}_0 \Delta\frac{v_w}{c} \approx \frac{1}{15000} \qquad (2)$$

which implies that a wind accuracy of 1m/s corresponds to a phase measurement accuracy of 1/15000 of a fringe (Rahnama, 2006).

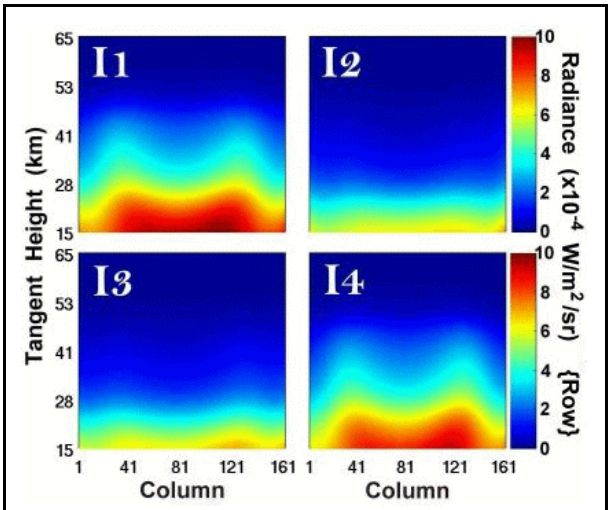

Fig 2: Examples of the interferograms for the four steps of the mirror. The steps are, clockwise from the upper left hand corner at 0, ~λ_o/4, ~λ_o/2 and ~3λ_o/4

A fringe is sampled by moving one of the Michelson mirrors to four positions such that the resulting path differences are separated by about a quarter wavelength (the mirror itself moves by about an eighth of a wavelength). These four interferograms (Fig 2) serve to describe the properties of the fringe from which the wind can be deduced. This process is know as phase stepping interferometry and more details can be found in Hariharan (1987, 1989), Shepherd et al (1985), Rahnama et al (2006), and Rochon et al (2006).

The mean value and total phase of interferogram, and line visibility are found from the four images. By removing the zero-wind phase, the phase due to Earth rotation and the phase induced by spacecraft motion from total phase, the Doppler phase is obtained, from which one obtains the line-of-sight (LOS) wind.

Description of the SWIFT Instrument

SWIFT has two fields of view (FOV) observing the limb at 48° and 132° with respect to the satellite forward direction for a coverage of 15 to 65km (Fig 3). A volume viewed by the forward FOV is sampled again about 9 minutes later by the aft FOV for a satellite at 650km. The fore and aft viewing angles are chosen such that the sampled volume is viewed from orthogonal directions.

Each field of view is defined by a reflecting telescope and a field stop in the fore and aft optical channels. The incoming radiation is directed by mirrors through the narrow-band Fabry-Perot etalon and bandpass filters to partially isolate the target O_3 line ($\tilde{\upsilon}_o$ = 1133.4335(cm^{-1})). The fields of view are

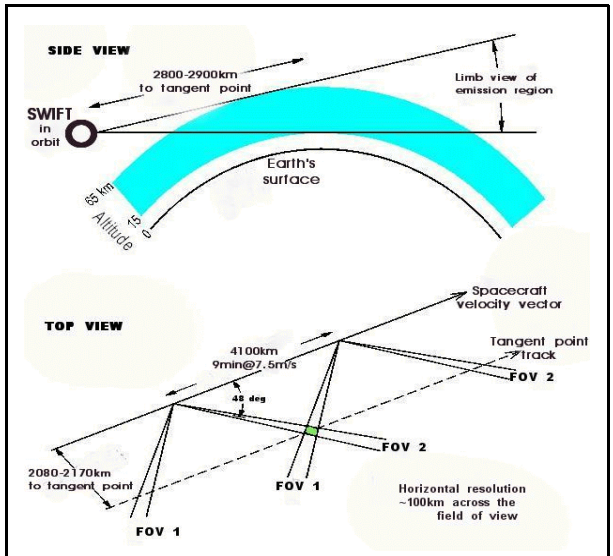

Fig 3: SWIFT field of views as seen from the side and from above the satellite.

combined and passed through a field-widened Michelson interferometer where it is modulated and then projected onto a two dimensional detector array. The array is 162x162 pixels split into two regions (81x162 pixels) assigned to each FOV.

Calibration is achieved by viewing blackbody sources, space and ammonia sources. More details of this and similar designs may be found in Rowlands et al, (1996), Scott et al (2000), Gault (2001) and Rahnama et al (2006). Calibration issues are discussed in Gault et al (2002) and more recently Rahnama et al (2005).

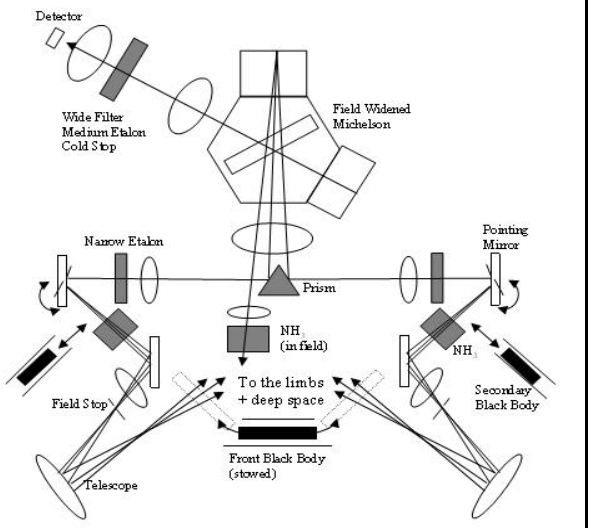

Fig 4: Schematic of the SWIFT instrument

The two dimensional detector array records an interferogram. The optics lines up the image such that the central incoming limb radiances lie on along a line of pixels. By definition, the limb radiances are mapped to the central column of the image from the top of the atmosphere (TOA) down from about 65km to 15km (rows 81 to 1). Each row of pixels contain similar limb radiances from either side of central "scan" for a total of 162 columns (Fig 2). For the moment, it is assumed that there is no significant curvature to the sides.

Line-of-sight Wind Recovery

The purpose of SWIFT is to measure winds, thus it is useful to briefly discuss the wind recovery. For wind measurements made by satellite instruments, the relative velocity of the source and the instrument is determined by a combination of Earth rotation, satellite motion, and the motion of the emitting volume of atmosphere (wind). Each of these three causes a shift in the wavenumber of the spectra and consequently induces a phase shift in the interferogram in addition to the instrument intrinsic phase.

The pixel interferogram intensity for the pixel at column i and row j of the detector can be written in terms of instrument visibility, U , line visibility, V, the mean value of the interferogram, I^{mean}, the total instrument phase of the interferogram, Φ, and the mirror phase, $\varphi_{k,}$ as:

$$I_{ijk} = I_{ij}^{mean} (1 + U_{ij} V_{ij} \cos(\Phi_{ij} + \varphi_{ijk})) \quad (3)$$

The total instrument phase is the sum of: the phase induced by spacecraft motion, φ_s, the phase induced by the Earth's rotation, φ_r, the phase due to wind, φ_w, and the intrinsic instrument phase φ_0 (phase of the interferogram in the absence of any relative motion between the emitting species & instrument).

$$\Phi_{ij} = \varphi_{0ij} + \varphi_{sij} + \varphi_{rij} + \varphi_{wij} \quad (4)$$

For the 4-point sampling (Fig 5), Eq 3 becomes a set of 4 equations with 3 unknowns, where I_{1ij}, I_{2ij}, I_{3ij} and I_{4ij}, are the measured radiances, φ_{1ij}, φ_{2ij}, φ_{3ij} φ_{4ij} are the Michelson phase steps, and U_{ij} which is part of the instrument characterization.

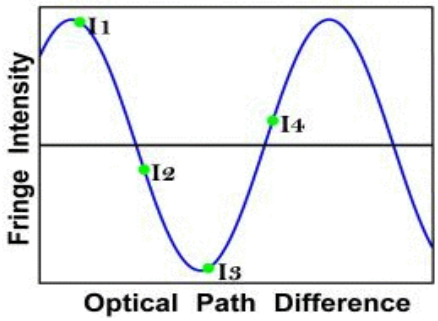

Fig 5: Four point measurement on a pixel's interferogram.

In practice, the mirror may not step in exactly $\pi/2$ intervals. To account for this each pixel interferogram is expressed as a three term truncated Fourier series. The three Fourier coefficients (J1, J2 and J3) are determined by fitting the four pixel intensities. The mean value of the interferogram, the total phase of the interferogram and the line visibility are obtained from the Fourier coefficients. The phase due to the wind is obtained by removing the earth rotation and satellite phase and the instrument phase from the total phase, and the line-of-sight wind is found by:

$$v_{ij} = \frac{c\,(\tan^{-1}(J_{3_{ij}}/J_{2_{ij}}) - \varphi_{rij} - \varphi_{sij} - \varphi_{0ij})}{2\,\pi\,\tilde{\nu}_o\,\Delta_{ij}^{eff}} \qquad (5)$$

A more detailed description of this procedure may be found in Shepherd et al (1993), Rochon (2000) and Rahnama (2006)

FORWARD MODEL

The forward model simulates a SWIFT radiance image, that is—

$$I_{ijk} = \int_{\Delta\tilde{\nu}} \Re_{ij}(\tilde{\nu}_w)\ \Im_{ijk}(\tilde{\nu}_s)\,d\tilde{\nu} \qquad (6)$$

where $\Re$ is the atmospheric line-of-sight emission and $\Im$ is the instrument function.

The atmospheric limb emission along the line of sight path, defined by x, is:

$$\Re_j(\tilde{\nu}_w) = \int_{\Delta x} B(\tilde{\nu}_w, T(x))\,d\Im(\tilde{\nu}_w, x) \qquad (7a)$$

where
$$\Im(\tilde{\nu}, x) = EXP\left(-\sum_{i=1}^{N}\int_{u_{space}}^{u_{SWIFT}} k_i(\tilde{\nu}, p(x), T(x)\,u(x))\,du(x)\right) \qquad (7b)$$

where B is the Planck function, p, T and u are the pressure, temperature and absorber amount as a function of x, the limb path variable, $\Im$ is the transmittance function from x to the instrument, k is the absorption coefficient and $\tilde{\nu}_w$ is a shifted wavenumber due to the wind (also a function of x).

The FLBL's atmospheric model is assumed to be locally spherically homogenous and refracting. It is also assumed that there are no significant sources outside the atmosphere. Refraction pulls the tangent point down, by as much as ⅓ km in the 1133(cm^{-1}) region. The layering of the atmosphere is designed such that

each tangent point, after adjusting for refraction, is situated on a level. There are 81 pixels in the vertical direction that map to 81 tangent heights from 15 to 65km in the atmosphere. The distance between tangent heights is about 630m. An additional 24 layers extend the atmosphere to TOA. The number of cells in a LOS path varies from 49 to 209 for tangent heights of 65 and 15 respectively. For convenience the tangent layer is split into two at the tangent point. The mean layer pressure and temperature used to evaluate the layer's absorption coefficient and the absorber amount used to calculate the layer optical depth are calculated by sub-dividing a layer into sublayers and calculating the weighted quantity with respect to absorber amount along the path within the layer. More details of the model can be found in Turner, 2005.

The instrument function at each pixel (*i,j*) and mirror step *k*, (eg: Rahnama et al, 2006) is simulated by

$$\mathfrak{B}_{ijk}(\tilde{\nu}_s) = R_{ij}(\tilde{\nu}_s)\, f_{ij}(\tilde{\nu}_s) \left[1 + U_{ij}(\tilde{\nu}_s) \cos\left(\Phi_{ij}(\tilde{\nu}_s) + \varphi_{ijk}(\tilde{\nu}_s) \right) \right] \qquad (8)$$

where $R_{ij}(\tilde{\nu}_0)$ is the instrument responsivity, f_{ij} is the pixel filter function (etalons, broadband pass filters, mirrors, etc...), and $\tilde{\upsilon}_s$ is a shifted wavenumber. The Doppler shift due to the satellite velocity and the earth's rotation velocity is accounted in $\tilde{\nu}_s$. This implies that the filter functions will shift slightly (in wavenumber space) with satellite position (unlike ordinary radiometers where the filter function may be considered invariant), a consideration that must be taken into account, if necessary, when constructing an operational model.

Each pixel on the interferogram is, in effect, a separate channel, meaning that SWIFT has potentially 162x81 channels per FOV. A line-by-line (LBL) radiative transfer model is an ideal method for evaluating interferogram, however it is generally too slow for operational purposes. Usually a parameterized model such as RTTOVS (Saunders et al, 1999) is employed.

Regression models generally operate on fixed vertical grids (i.e. pressure). In this circumstance, the fixed grid is a disadvantage for limb scanning where the instrument is pointing at a specific point in the atmosphere relative to the satellite. The tangent point will move constantly about relative to either the actual surface or a constant pressure surface, hence a series of interpolations would be required to use a fixed grid, adding to the errors. Regression model parameters might be a problem as well. RTTOVS, for example, requires 34 parameters per level per channel for its regression model. This model simulates nadir paths. Limb paths are much more optically thick than nadir paths and experience indicates that more model parameters would are likely to be required for longer paths in order to maintain accuracy. A regression model usually calculates an independent mean spectral transmittance for variable absorbers and sometimes combines absorbers of near negligible variability, effectively ignoring spectral line overlap which might be a problem if high accuracy is required.

Although a traditional LBL model is usually considered to be slow for operational uses, it has the advantages of not being constrained by fixed grids, accounts for line overlap and any other wavenumber dependent variables. The fast line-by-line (FLBL) radiative transfer model (Turner, 1995, 2005) is exactly like an LBL

model except that it uses absorption coefficient lookup tables (k-table) and a bicubic interpolator to replace the time consuming part of an LBL code that calculates absorption coefficients directly from a spectral database. This "replacement" typically speeds up an LBL by almost two orders of magnitude (Turner, 1995). Normally the FLBL would not be suitable because of the large size of the k-tables, however SWIFT's spectral region is fairly narrow (~1.2(cm^{-1})) thus reducing the tables to a manageable size.

A regression model similar to RTTOVS would require some additional parameters to account for the atmospheric winds and to account for possible wavenumber shifts of the filters, in any. This would require experimentation with an LBL to identify these parameters and any other potential problems, for example spectral overlap. With this in mind it was decided to optimize the FLBL and use it to access the feasibility of assimilating winds into the NWP and possibly optimize it for operational use.

The FLBL was reconfigured to simulate the SWIFT interferograms. Only one major change was introduced to the basic FLBL model to improve speed. Since the spectral region is fairly narrow the explicit Planck function for each layer is replaced by a simple linear function. This substitution realizes a gain of about 2% in execution speed.

For this study, seven absorbers (H_2O, O_3, N_2O, CH_4, NH_4, CFC12 & CFC22) are considered and eight k-tables were constructed spanning 1.2(cm^{-1}) (the nominal full width of the filter response functions) at a spectral resolution of .0001(cm^{-1}). Two are required for water vapour (Turner, 1995). These tables formed a reference set.

The preliminary work by Rochon et al (2006) and Rahmana et al (2006) was done using a local LBL (Rochon, private communication) and a variant of FASCATM (Gallery et al, 1983), thus it was prudent to compare the FLBL with the local LBL. The spectrally integrated limb emissions (neglecting the instrument function, $\mathfrak{Z}$) for many limb paths and spectral resolution were compared. Figure 6 shows sample results of the difference between the two codes for tangent heights of 15, 31 and 58 km at spectral resolutions of 0.0005 and 0.005 (cm^{-1}). In general, the models agree. There is a small background difference at lower tangent heights which are probably due to the difference in the number of contributing lines to $k(\tilde{\nu})$. The FLBL considered spectral lines out to 100(cm^{-1}) from $\tilde{\nu}$, whereas the local LBL used lines out to 10(cm^{-1}) away. There are also missing lines which may be attributed to the use of different versions of the HITRAN database (Rothman et al, 2003). It is safe to assume that the FLBL is a viable faster alternative to the local LBL code.

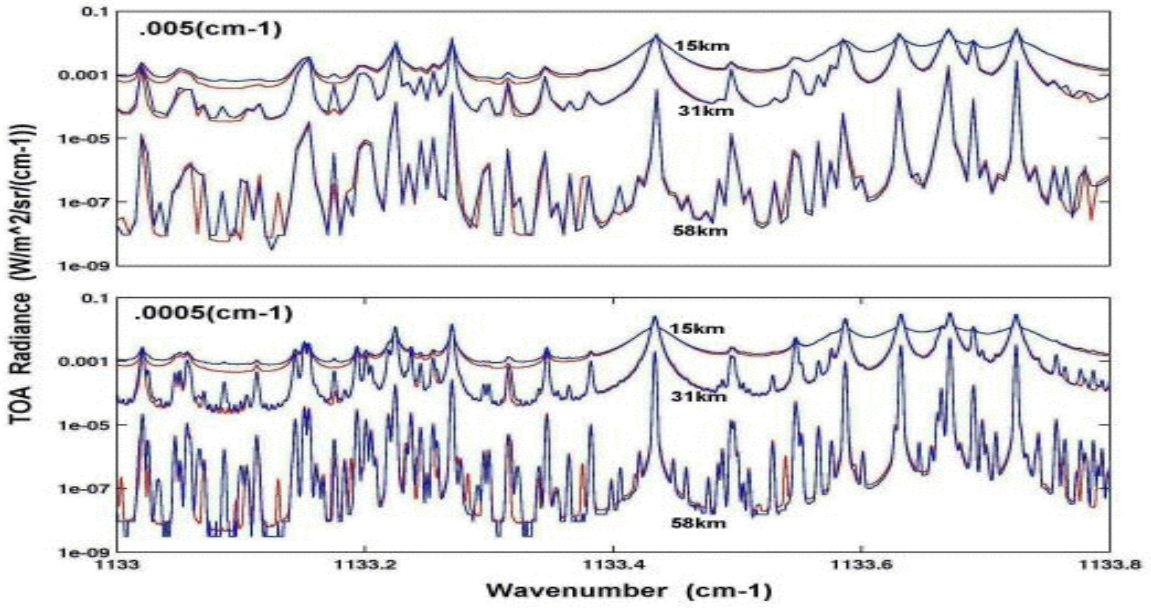

Fig 6: Comparison between the local LBL (—) and the FLBL (—). Comparisons are shown for three limb views (tangent height= 58, 31 & 15km).

Impact on the Doppler Wind Due to Spectral Resolution

A high resolution FLBL is better than a low one, however the computational expense increases with resolution (Fig 7). In terms of efficiency a low resolution model is ideal, but how does the spectral resolution impact on the derived winds?

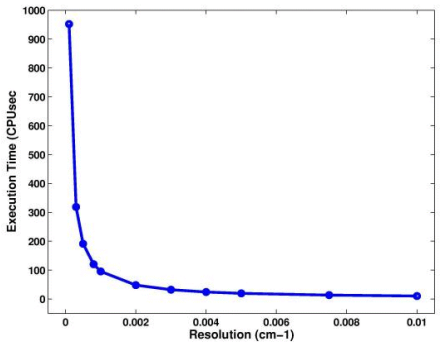

Fig 7: FLBL execution times as a function of spectral resolution.

One method is to simulate the four interferograms using Eq 6 and then to evaluate the LOS winds from Eq 5 for various resolutions and compare the results to a reference. For simplicity the atmospheric winds are set to zero and the reference resolution is the highest, .0001(cm^{-1}).

Ideally the difference should be zero, however errors will arise due to the fitting of the truncated Fourier series and due to Eq 5 being derived from a mean, i.e. a reference wavenumber. An acceptable spectral resolution is one where the difference in the winds derived from a lower resolution model and the reference is below some tolerance level.

Figure 8 shows the difference, D, between the wind evaluated at .0001(cm^{-1}) and various resolutions up to .01(cm^{-1}). Up to .001(cm^{-1}) the differences are negligible across the entire FOV. At .002(cm^{-1}) non-negligible differences start to appear in the upper atmosphere off to the sides of the FOV. By .005(cm^{-1}) the differences are no longer acceptable. It appears that it may be necessary to use a resolution of .002(cm^{-1}) or possibly .003(cm^{-1}), if the outer columns of the image are discarded. The latter would be three times faster.

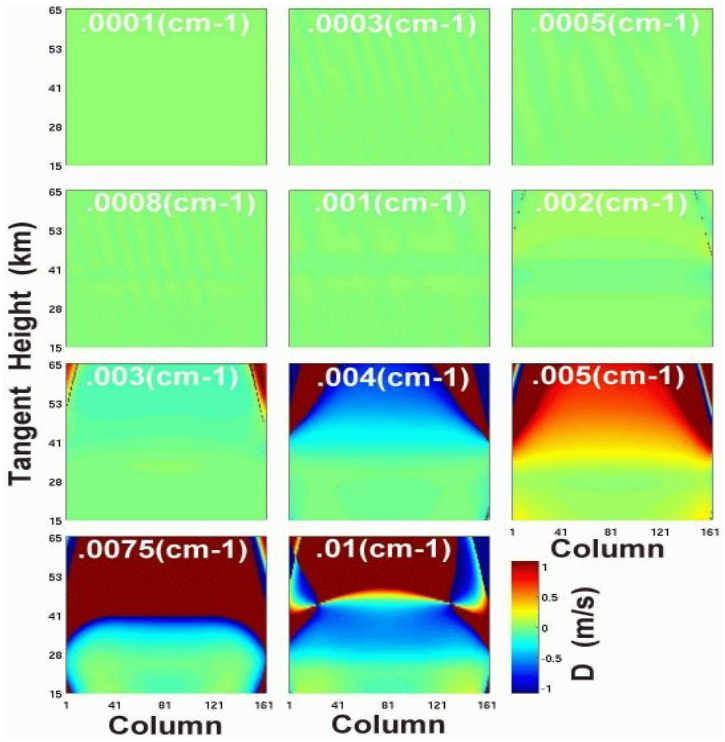

Fig 8: Difference, D, in wind derivation between the highest and the lower resolution FLBLs.

The primary purpose of subdividing a layer is to account for physical path length due to refraction. The previous calculation assumed 20 sublayers per layer, that is—a sublayer is typically 31m. Figure 9 illustrates the choice of sublayers, relative to a choice of 20 sublayers, on the impact on the winds. The results indicate that only 8-10 sublayers are required to minimize the impact of estimating the path length through the layer. As before if the outer columns of the interferogram are excluded then the number can be reduced to 6 or 7 sublayers per layer.

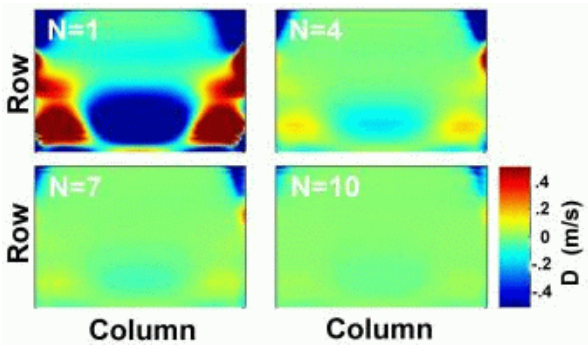

Fig 9: Impact on the choice of the number of sub-layers in a layer.

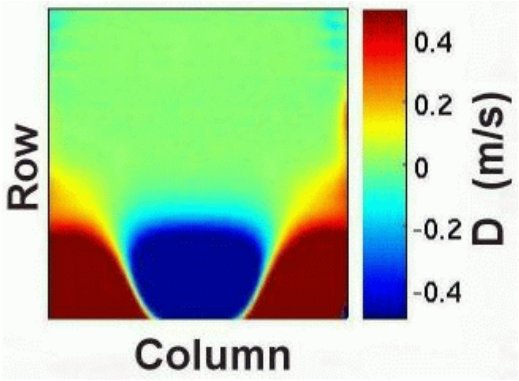

Fig 10: Impact of excluding refraction

Figure 10 illustrates the impact of ignoring refraction, which clearly must be included, especially in the lower altitudes.

Discussion

The chosen preliminary forward model for SWIFT is the FLBL which has been modified to include the instrument function described in Rochon et al (2006) and Rahnam et al (2006). To date the program has been optimized to execute as quickly as possible and with as little memory as possible on a LINUX operating within an Intel architecture. On this system one complete interferogram (.002 (cm^{-1})) takes about 40CPUsec. It remains to be seen how much faster the FLBL is once it is optimized to run on the IBM cluster. (The Atmospheric Science and Technology Branch operates their NWP on a IBM cluster of p690s and allows for parallel processing). In the event that a parameterized model approach needs to be taken, the FLBL model will be useful to build a database from which to derive the coefficients of the parameterized model.

The wind impact studies indicate that if the outer 20 columns from both sides of the interferogram are discarded then a lower resolution and fewer sub layers could be used. This could result in a model that is 3 or 4 times faster.

The testing and optimizing the FLBL model is not complete. The winds will also be affected by how well the spectroscopy and the distribution of an absorber are known. The ozone line at 1133(cm^{-1}) was originally chosen because it is relatively isolated, that is— it is in a region where there are few significant absorbers, thus reducing the amount of information required to simulate the signal accurately. It may be possible to combine the small but significant absorbers in some way (eg; like the uniformily mixed absorbers in RTTOVS) which would decrease execution time significantly. In addition, the gradient portion still has to be completed and tested. Once completed and tested the model will be integrated into a data assimilation system to determine if it is feasible to assimilate SWIFT data into the numerical weather prediction model and to what degree it impacts the forecast. If it turns out that the FLBL is too slow on the IBM cluster, then efforts will turn to a parameterized model. Any parameterized model will benefit from the work done with the FLBL.

Finally, the flight version of the instrument is not yet finalized. Some of the instrument and measurement parameters still have to be optimized and consequently the algorithm might have more room be refined in order to reduce the wind errors to better than 3 ms^{-1} for 20 to 45 km and to better than 5 ms^{-1} for the extended range of 15 to 55 km through the entire life of the mission

Acknowledgments

The SWIFT project is supported by the Canadian Space Agency (CSA). SWIFT also received support from Natural Sciences and Engineering Research Council of Canada (NSERC), and during the phase A study from the European Space Agency (ESA) and the Center for Research in Earth and Space Technology (CRESTech).

References

Gallery, W.O., F.X. Kneizys and S.A. Clough, 1983: Air Mass Computer Program for Atmospheric Transmittance/Radiance Calculations: FSCATM. *Air Force Geophysics Laboratory Tech. Rep. AFGL-TR-83-0065*, 145pp.

Gault, W.A., I.C. McDade, Y.J. Rochon and A. Scott, 2002: Filters and calibration for the SWIFT instrument on GCOM-A1, *Proc. 9th Int Symp on Remote Sensing, Sensors, Systems and Next-Generation Satellites VI*, Aghia Pelagia, Crete, Greece, The International Society for Optical Engineering (SPIE), **4881**, pp60-66..

Gault, W.A., I.C. McDade, G.G. Shepherd, R. Mani, S. Brown, P. Gregory, A. Scott, Y.J. Rochon and W.F.J. Evans, 2001: SWIFT: an infrared Doppler Michelson interferometer for measuring stratospheric winds, *Proc. 8th Int Symp on Remote Sensing, Sensors, Systems and Next-Generation Satellites V*, Toulouse, France, The International Society for Optical Engineering (SPIE), **4540**, pp476-481.

Hariharan, P., 1987: Digital phase-stepping interferometry: effects of multiply reflected beams. *Appl. Opt.,* **26**, pp2506-2507

Hariharan, P., 1989: Phase-stepping interferometry with laser diodes, 2: Effects of laser wavelength modulation. *Appl. Opt.* **28**(10), pp1749-1750.

McDade, I.C., G.G. Sheperd, W.A. Gault, Y.J. Rochon, C. McLandress, A. Scott, P. Gregory, N. Rowlands, G. Buttner, T. Wehr, J.L. Bezy, 2002: Stratospheric Wind Measurements with SWIFT onboard GCOM-A1, *Proceedings of International Symposium on Stratospheric Variations and Climate*, Fukuoka, Japan, 12-15 November, 2002.

Ortland, D.A., W.R. Skinner, P.B. Hays, M.D. Burrage, R.S. Lieberman, A.R. Marshallm and D.A. Gell, 1996: Measurements of stratospheric winds by the High Resolution Doppler Imager, *J. Geophys. Res.*, **101**, 10351-10363

Rahnama, P., Y.J. Rochon, I.C. McDade, G.G. Shepherd, W.A. Gault and A. Scott, 2006: Satellite Measurement of Stratospheric Winds and Ozone Using Doppler Michelson Interferometry, Part I: Instrument Model and Measurement Simulation, *JAOT*, **23**, pp753-769.

Rahnama, P., I.C. McDade, A. Scott and Y.J. Rochon, 2005: Simulations of on-board calibration procedures for the SWIFT instrument. *European Geosciences Union (EGU) General Assembly*, Vienna, Austria, 24-29 April 2005. Geophysical Research Abstracts (GRA) Space Instrumentation, **7**, 01411.

Rochon, Y.J., P. Rahnama and I.C. McDade, 2006: Satellite Measurement of Stratospheric Winds and Ozone Using Doppler Michelson Interferometry, Part II: Retrieval Method and Expected Performance, *JAOT*, **23**, pp770-784.

Rochon, Y.J., 2000: The retrieval of winds, Doppler temperatures, and emission rates for the WINDII experiment. Ph.D. dissertation, York University, Toronto, Canada, 474pp.

Rothman, L.S., A. Barbe, D. Chris Benner, L.R. Brown, C. Camy-Peyret, M.R. Carleer, K. Chance, C. Clerbaux, V. Dana, V.M. Devi, A. Fayt, J.-M. Flaud, R.R. Gamache, A. Goldman, D. Jacquemart, K.W. Jucks, W.J. Lafferty, J.-Y. Mandin, S.T. Massie, V. Nemtchinov, D.A. Newnham, A. Perrin, C.P. Rinsland, J. Schroeder, K.M. Smith, M.A.H. Smith, K. Tang, R.A. Toth, J. Vander Auwera, P. Varanasi, and K. Yoshino., 2003: The HITRAN molecular spectroscopic database: edition of 2000 including updates through 2001, *J.Q.S.R.T.,* **82**, 5-44.

Rowlands, N., G.J. Buttner, A. Raab, G.G. Shepherd, W.A. Gault, M.W. Cann, S. Dobbie, S. Sargoytchev, W.E. Ward, and D.W. Tarasick, 1996: A satellite instrument to measure stratospheric winds, *Proc. SPIE on Optical Spectroscopic Techniques and Instrumentation for Atmospheric and Space Research II*, Denver, Colorado, USA, The International Society for Optical Engineering (SPIE), **2830**, pp2-14.

Saunders, R., M. Matricardi and P. Brunel, 1999. An Improved Fast Radiative Transfer Model for Assimilation of Satellite Radiance Observations. *Appl. Opt.*, **34**, 8396-8399.

Scott, A., N. Mackay, S. Wang, N. Rowlands, G.G. Shepherd, W. Gault, I.C. McDade and Y.R. Rochon, 2000: The SWIFT instrument, *Proc. SPIE on Optical remote sensing of the atmosphere and clouds II*, Sendai, Japan, The International Society for Optical Engineering (SPIE), **4150**, pp420-426.

Shepherd, GG, W. A. Gault, D. W. Miller, Z. Pasturczyk, S. F. Johnston, P. R. Kosteniuk, J. W. Haslett, D. J. W. Kendall and J.R. Wimperis, 1985: WAMDII: wide-angle Michelson Doppler imaging interferometer for Spacelab, *Appl. Opt.* **24**, 1571-1584.

Shepherd, G.G., G. Thuillier, W.A. Gault, B.H. Solheim, C. Hersom, J.M. Alunni, J.F. Brun, S. Brune, P. Charlot, D.L. Desaulniers, W.F.J. Evans, F. Girod, D. Harvie, R.H. Hum, D.J.W. Kendall, E.J. Llewellyn, R.P. Lowe, J. Ohrt, F. Pasternak, O. Peillet, I. Powell, Y. Rochon, W.E. Ward, R.H. Wiens and J. Wimperis, 1993: WINDII - The wind imaging interferometer on the upper atmosphere research satellite. J. Geophys. Res., **98**, 10,725-10,750.

Turner, D.S. 1995: Absorption Coefficient Estimation Using A Two Dimensional Interpolation Procedure, *J.Q.S.R.T.*, **53**(6), 633-637.

Turner, D.S., *The Gradient Fast Line-by-Line Model*, Technical Proceedings of the Fourteenth International ATOVS Study Conference, Beijing, China, 25 - 31 May 2005.

INTERNATIONAL ATOVS WORKING GROUP

Sharing ideas, plans and techniques

to study the earth's weather

using space-based observations

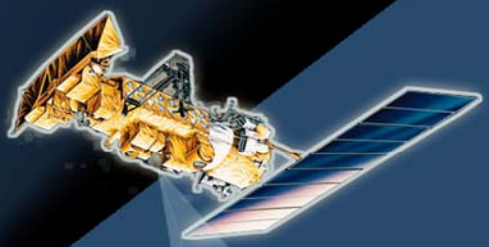

Proceedings of the Fifteenth International TOVS Study Conference

Maratea, Italy

4 October - 10 October 2006

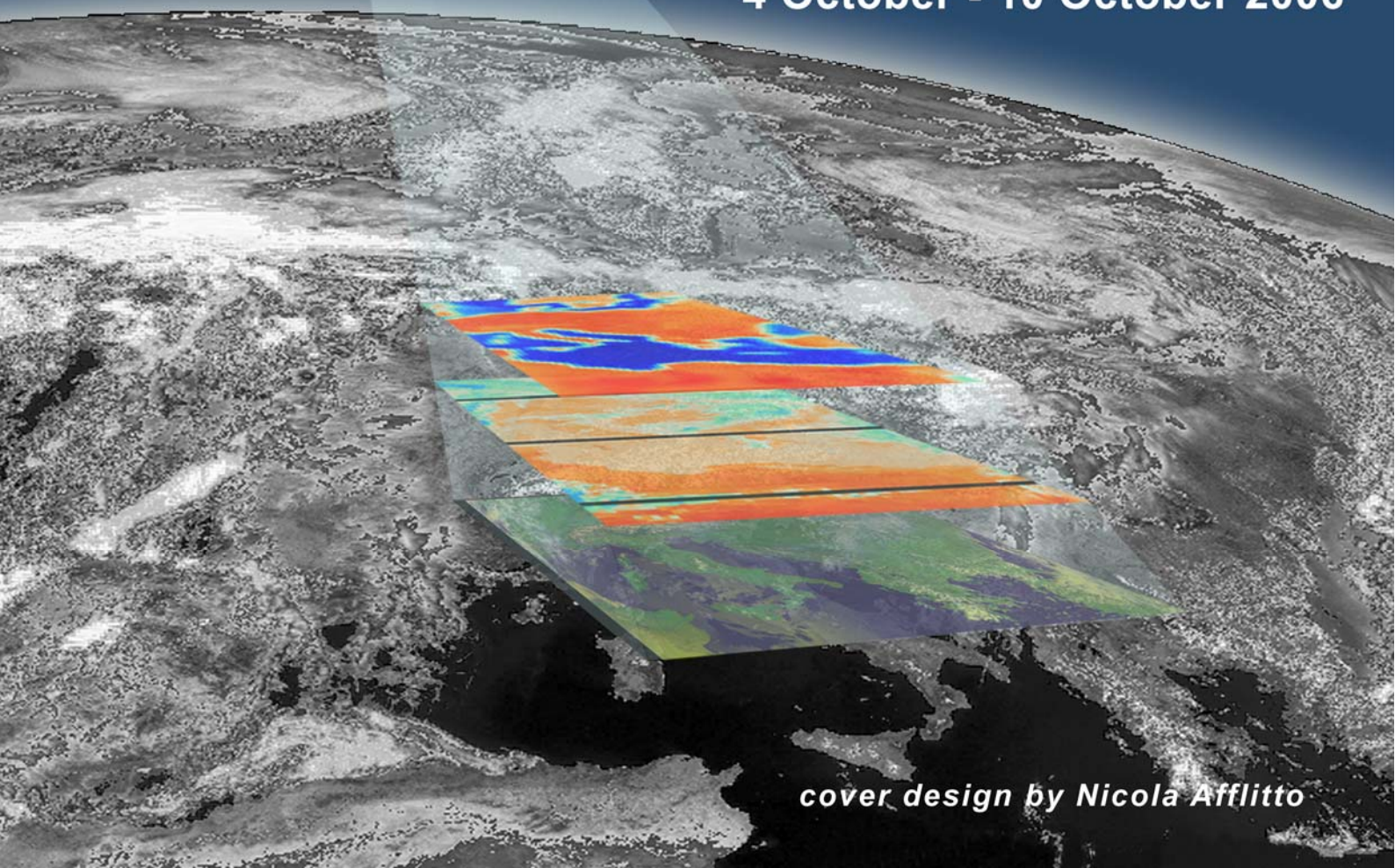

cover design by Nicola Afflitto